A&A 528, A57 (2011)
DOI: 10.1051/0004-6361/201014899

Astronomy & Astrophysics

Infrared emission from the composite grains: effects of inclusions and porosities on the 10 and 18 μm features

D. B. Vaidya[1] and R. Gupta[2]

[1] ICCSIR, 380009 Ahmedabad, India
e-mail: deepak.vaidya@iccsir.org
[2] IUCAA, Post Bag 4, Ganeshkhind, 411007 Pune, India
e-mail: rag@iucaa.ernet.in

Received 30 April 2010 / Accepted 6 January 2011

ABSTRACT

Aims. In this paper we study the effects of inclusions and porosities on the emission properties of silicate grains and compare the model curves with the observed infrared emission from circumstellar dust.
Methods. We calculated the absorption efficiency of the composite grain, made up of a host silicate oblate spheroid and inclusions of ice/graphite/or voids, in the spectral region 5.0–25.0 μm. The absorption efficiencies of the composite spheroidal oblate grains for three axial ratios were computed using the discrete dipole approximation (DDA). We studied the absorption as a function of the volume fraction of the inclusions and porosity. In particular, we studied the variation in the 10 μm and 18 μm emission features with the volume fraction of the inclusions and porosities. We then calculated the infrared fluxes for these composite grains at several dust temperatures (T = 200−350 K) and compared the model curves with the average observed IRAS-LRS curve, obtained for circumstellar dust shells around oxygen rich M-type stars. The model curves were also compared with two other individual stars.
Results. The results for the composite grains show variation in the absorption efficiencies with the variation in the inclusions and porosities. In particular, it is found that the wavelength of peak absorption at 10 μm shifts towards longer wavelengths with variation in the volume fraction of the graphite inclusions. The spheroidal composite grains with axial ratio ~1.33; volume fraction of f = 0.1, and dust temperature between 210–340 K, fit the observed infrared emission from circumstellar dust reasonably well in the wavelength range 5–25 μm. The model flux ratio, R = Flux(18 μ)/Flux(10 μ), compares well with the observed ratio for the circumstellar dust.
Conclusions. The results on the composite grains clearly indicate that the silicate feature at 10 μm shifts with the volume fraction of graphite inclusions. The feature does not shift with the porosity. Both the features do not show any broadening with the inclusions or with porosity. The absorption efficiencies of the composite grains calculated using DDA and effective medium approximation (EMA) do not agree. The composite grain models presented in this study need to be compared with the observed IR emission from the circumstellar dust around a few more stars.

Key words. dust, extinction – circumstellar matter

1. Introduction

Circumstellar dust grains are most likely nonspherical, porous, fluffy, and composites of many small grains glued together, owing to grain-grain collisions, dust-gas interactions and various other processes. Since there is no exact theory to study the scattering properties of these inhomogeneous grains, there is a need for formulating models of electromagnetic scattering by these grains. There are two widely used approximations for studying the optical properties of composite grains: effective medium approximation (EMA) and discrete dipole approximation (DDA). We use DDA for calculating the absorption efficiencies of the composite grains. Mathis & Whiffen (1989) and Mathis (1996) have used EMA to calculate the absorption cross-section for the composite grains containing silicate and amorphous carbon. For details on EMA refer to Bohren & Huffman (1983) and for DDA refer to Draine (1988). For a comparison of the two methods, see Bazell & Dwek (1990), Perrin & Lamy (1990), Perrin & Sivan (1990), Ossenkopf (1991), Wolff et al. (1994), and Iati et al. (2004).

In this paper we study the effects of inclusions and porosities on the absorption efficiencies of the silicate grains in the wavelength range of 5–25 μm. In particular we study the variation in the emission features at 10 μm and 18 μm with the volume fraction of inclusions and porosities. We use these absorption efficiencies to compare the average observed infrared emission curve obtained for the circumstellar dust around several oxygen-rich M-type stars (IRAS LRS catalog of Olnon & Raimond 1986). We have also compared the model curves with two individual stars.

Earlier studies by Henning & Stognienko (1993) have shown that composite oblate grains containing silicates and graphites did not show any changes in 10 μm and 18 μm features or the ratio R = Flux(18 μ)/Flux(10 μ) with respect to the silicate grains. It must be noted here that they used DDA for calculating absorption cross-section of the composite oblate grains. O'Donnell (1994) also did not find any shift in the 10 μm or 18 μm features for the grains containing silicates with the inclusions of carbons (glassy and amorphous). Min et al. (2006, 2007) have used DDA to study the composite and aggregated silicates and found that the 10 μm feature shifts to the shorter wavelengths. Jones (1988) found enhancement in the infrared absorption features at 9.7 μm and 18 μm for porous silicate grains and hollow spheres. In view of these studies a detailed investigation of the 10 μm and 18 μm features using realistic grain models is called for.

In Sect. 2 we give the validity criteria for the DDA and the composite grain models. In Sect. 3 we present the results of our

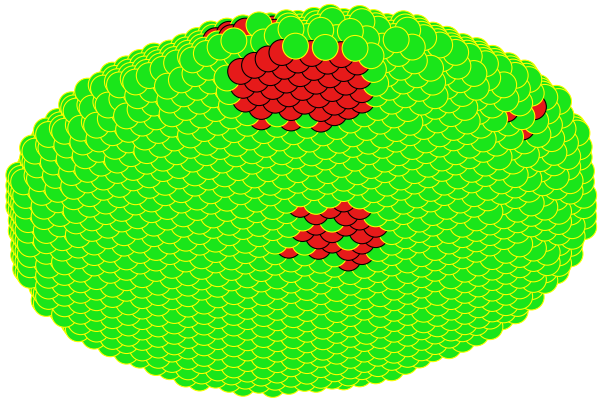

Fig. 1. A composite grain with a total of $N = 9640$ dipoles. The inclusions are embedded in the host oblate spheroid (in red).

computations and compare the model curves with the observed IR fluxes obtained by IRAS satellite. Section 4 provides a detailed discussion of the comparison of our model/results with available model/results from other authors. The main conclusions of our study are given in Sect. 5.

2. Composite grains and DDA

We used the modified computer code (Dobbie 1999) to generate the composite grain models used in the present study. We studied composite grain models with a host silicate oblate spheroid containing $N = 9640$, 25 896 and 14 440 dipoles, each carved out from $32\times24\times24$, $48\times32\times32$ and $48\times24\times24$ dipole sites, respectively; sites outside the spheroid are set to be vacuum and sites inside are assigned to be the host material. It is to be noted that the composite spheroidal grain with $N = 9640$ has an axial ratio of 1.33, whereas $N = 25\,896$ has the axial ratio of 1.5, and $N = 14\,440$ has the axial ratio of 2.0. The volume fractions of the graphite inclusions used are 10%, 20%, and 30% (denoted as $f = 0.1$, 0.2, and 0.3). Details on the computer code and the corresponding modification to the DDSCAT code (Draine & Flatau 2003) are given in Vaidya et al. (2001, 2007) and Gupta et al. (2006). The modified code puts out a three-dimensional matrix specifying the material type at each dipole site, and the sites are either silicate, graphite, or vacuum. An illustration of a composite spheroidal oblate grain with $N = 9640$ dipoles is shown in Fig. 1. This figure also shows the inclusions embedded in the host oblate spheroid. Oblate spheroids were selected based on the numerous results of previous studies (Greenberg & Hong 1975; Henning & Stognienko 1993; O'Donnell 1994; Gupta et al. 2005) that showed that oblate spheroids represent properties of circumstellar dust particles better; specifically, this model provides a good fit to the observed polarization across the 10 μm feature (Lee & Draine 1985).

There are two validity criteria for DDA (see e.g. Wolff et al. 1994). (i) $|m|kd \leq 1$, where m is the complex refractive index of the material, $k = \pi/\lambda$ the wave number, and d the lattice dispersion spacing; and (ii) d should be small enough (N should be sufficiently large) to describe the shape of the particle satisfactorily. We have checked the validity criteria $|m|kd \leq 1$, for all the composite grain models with inclusions of ices, graphites, and voids. The $|m|kd \leq 1$ varied from 0.041 at 5 μm for $N = 9640$ to 0.001 at 25 μm for $N = 25\,896$.

Table 1 shows the number of dipoles (N) for each grain model in the first column and also the size of inclusion ("n" across the diameter of an inclusion, e.g., 152 for $N = 9640$, see Vaidya et al. 2001), the remaining three columns show the number of inclusions and number of dipoles per inclusion (in brackets) for the three volume fractions ($f = 0.1$, $f = 0.2$, and $f = 0.3$), respectively. The complex refractive indices for silicates and graphites were obtained from Draine (1985, 1987) and the one for ice is from Irvine & Pollack (1969).

Table 1. Size of inclusions, number of inclusion (and number of dipoles per inclusion).

Inclusions	Inclusion	Fractions	
$N = 9640$	$f = 0.1$	$f = 0.2$	$f = 0.3$
AR = 1.33	32/24/24		
$n = 16/12/12$	1(1184)	2(1184)	
$n = 8/6/6$	6(152)	11(152)	16(152)
$n = 4/3/3$	38(16)	76(16)	114(16)
$N = 25\,896$	$f = 0.1$	$f = 0.2$	$f = 0.3$
AR = 1.50	48/32/32		
$n = 12/8/8$	7(432)	13(432)	19(432)
$n = 6/4/4$	54(56)	108(56)	162(56)
$n = 3/2/2$	216(8)	432(8)	648(8)
$N = 14\,440$	$f = 0.1$	$f = 0.2$	$f = 0.3$
AR = 2.00	48/24/24		
$n = 16/8/8$	3(536)	6(536)	8(536)
$n = 12/6/6$	6(224)	11(224)	16(224)
$n = 8/4/4$	23(64)	46(64)	68(64)
$n = 6/3/3$	38(24)	76(24)	114(24)
$n = 4/2/2$	91(8)	181(8)	271(8)

As mentioned before, the composite spheroidal grain models with $N = 9640$, 25 896, and 14 440 have the axial ratio 1.33, 1.5, and 2.0 respectively and if the semi-major axis and semi-minor axis are denoted by $x/2$ and $y/2$, respectively, then $a^3 = (x/2)(y/2)^2$, where "a" is the radius of the sphere whose volume is the same as that of a spheroid. To study randomly oriented spheroidal grains, it is necessary to get the scattering properties of the composite grains averaged over all of the possible orientations. In the present study we used three values for each of the orientation parameters (β, θ and ϕ), i.e., averaging over 27 orientations, which we find quite adequate (see Wolff et al. 1994).

3. Results and discussion

3.1. Absorption efficiency of composite spheroidal grains

Recently, we have studied the effects of inclusions and porosities in the silicate grains on the infrared emission properties in the wavelength region 5–14 μm (Vaidya & Gupta 2009). Here, we study the absorption properties of the composite spheroidal grains with three axial ratios, viz. 1.33, 1.5, and 2.0, corresponding to the grain models with $N = 9640$, 25 896, and 14 440 respectively, for three volume fractions of inclusions, 10%, 20%, and 30%, in the extended wavelength region 5.0–25.0 μm. The selected inclusions are graphites, ices and voids. We particularly study the effects of inclusions and porosity on the 10 μm and 18 μm features individually, as well as on the flux ratio $R = \mathrm{Flux}(18\,\mu)/\mathrm{Flux}(10\,\mu)$.

Figures 2a–c show the absorption efficiencies ($Q_{\rm abs}$) for the composite grains with the host silicate spheroids containing 9640, 25 896, and 14 440 dipoles. The three volume fractions, 10%, 20%, and 30%, of ice inclusions are also listed in the top (a) panel. It is seen that there is no appreciable variation in the absorption efficiency with the change in the volume fraction of inclusions in the wavelength region 5–8 μm. The variation in the

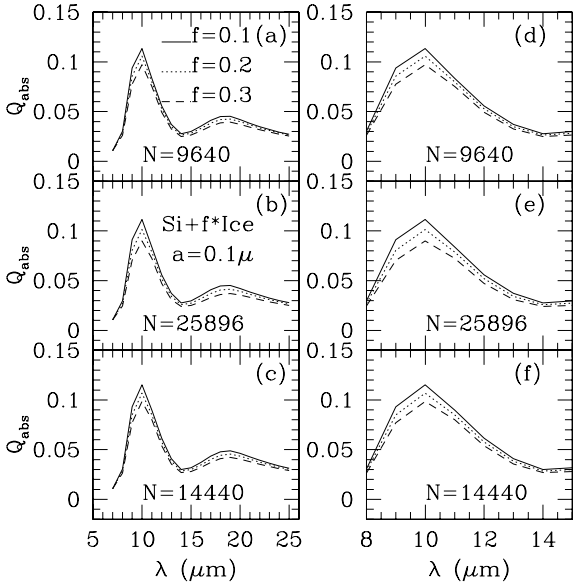

Fig. 2. Absorption efficiencies for the composite grains with host silicate spheroids and ices as inclusions for all three axial ratios N = 9640 (AR = 1.33), N = 25 896 (AR = 1.50), and N = 14 440 (AR = 2.00). The 10 μ feature is highlighted in the right side panels **d)–f)**.

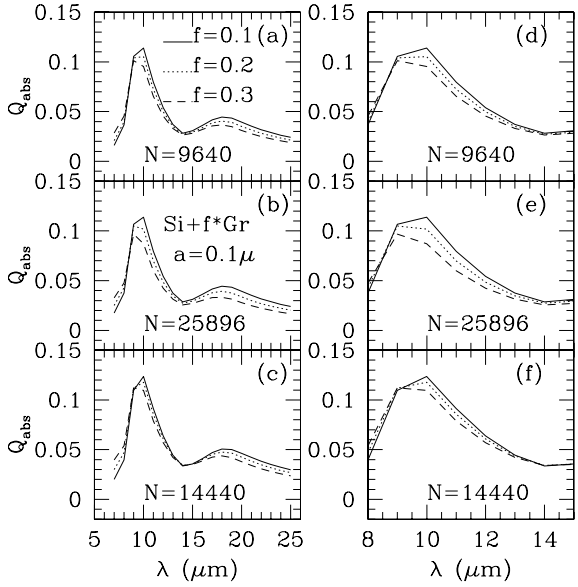

Fig. 3. Absorption efficiencies for the composite grains with host silicate spheroids and graphites as inclusions for all three axial ratios N = 9640 (AR = 1.33), N = 25 896 (AR = 1.50), and N = 14 440 (AR = 2.00). The 10 μ feature is highlighted in the right side panels **d)–f)**.

absorption efficiency is clearly seen in the wavelength range between 8–25 μm with peaks at 10 μm and 18 μm. It is also to be noted that there is no shift in the wavelength of the peak absorption. In Figs. 2d–f variation in the absorption efficiency between 8 and 14 μm is highlighted. It is seen that the strength of both absorption peaks decrease with the increase in the volume fraction of the inclusions.

Figure 3 shows the absorption efficiencies for the composite grains with the host silicate spheroids and graphite inclusions. It is seen in Figs. 3d–f that the 10 μ feature shifts towards shorter wavelengths as the volume fraction of the graphite inclusions increases. Ossenkopf et al. (1992) have studied the effects of inclusions of Al_2O_3, MgO, MgS, and carbons (glassy and amorphous) in the silicate grains, and they too have found that the 10 μm absorption feature shifts shortwards. O'Donnell (1994) did not find any shift in 10 μm feature for the silicate grains with the inclusions of carbons. We did not find any shift in the absorption feature at 18 μm with the change in the volume fraction of the graphite inclusions. Ossenkopf et al. (1992) and O'Donnell (1994) also did not find any variation in the 18 μm feature with the inclusions. Henning & Stognienko (1993) have used composite oblate spheroid grains containing silicates and graphites and find no significant shift in the 10 μm or 18 μm features. Results in Figs. 3a–f also indicate that absorption efficiency does not vary with the shape of the grains (axial ration AR = 1.33, 1.50, 2.00).

We went on to check the absorption efficiencies of the composite grains for several inclusion sizes (n) at a constant volume fraction. (See Table 1 e.g. for N = 9640, where the array 8/6/6 indicates the size of the inclusion.) We did not find any significant change in the absorption efficiency or any shift in the absorption features (Vaidya et al. 2001).

We compared our results on the absorption efficiencies of the composite grains obtained using the DDA with the results obtained using the EMA-T-matrix based calculations. The results with EMA are displayed in Fig. 4. For these calculations, the optical constants were obtained using the Maxwell-Garnet mixing

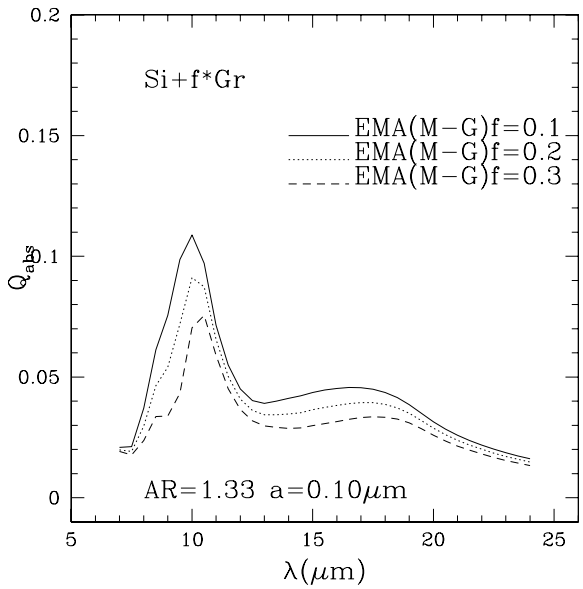

Fig. 4. EMA(M-G) calculations with AR = 1.33 and three volume fractions.

rule (i.e. effective medium theory, see Bohren & Huffman 1983). Description of the T-matrix method/code is given by Mishchenko et al. (2002).

In Fig. 5 we show the ratio Q(EMA)/Q(DDA) to compare the results obtained using both these methods. It is seen that the absorption curves obtained using the EMA-T matrix calculations deviate from the absorption curves obtained using the DDA, as the volume fraction of inclusions increases. The results based on the EMA-T-matrix calculations and DDA results do not agree because the EMA does not take the inhomogeneities within the grain into account (viz. internal structure, surface roughness, voids; see Wolff et al. 1994, 1998), and material interfaces and

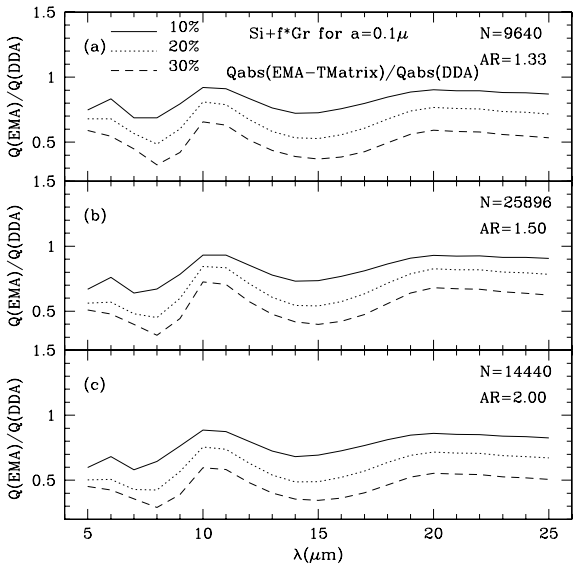

Fig. 5. Ratio for absorption efficiency using DDA and EMA.

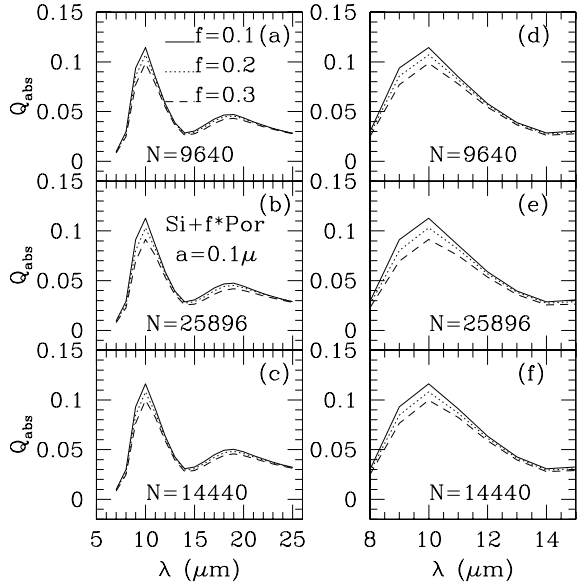

Fig. 6. Absorption efficiencies for the composite grains with host silicate spheroids and voids (vacuum) as inclusions for all three axial ratios N = 9640 (AR = 1.33), N = 25 896 (AR = 1.50), and N = 14 440 (AR = 2.00). The 10 μ feature is highlighted in the right side panels **d)–f)**.

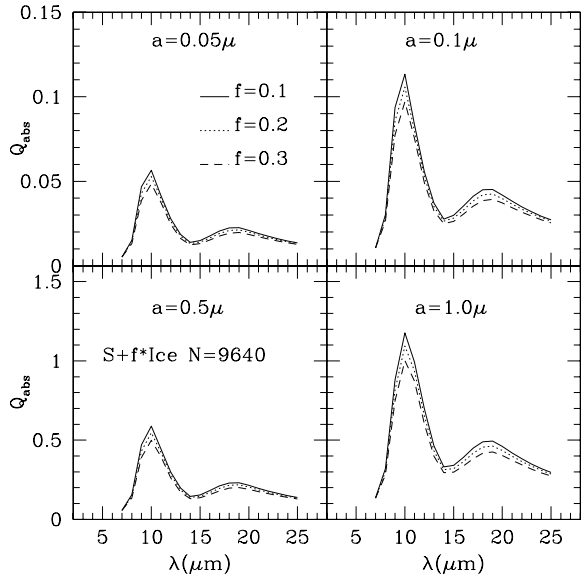

Fig. 7. Variation in absorption efficiencies with composite grains sizes. Host silicate spheroids contain dipoles N = 9640 and ices as inclusions.

shapes are smeared out into a homogeneous "average mixture" (Saija et al. 2001). However, it would still be very useful and desirable to compare the DDA results for the composite grains with those computed by other EMA/Mie type/T matrix techniques in order to examine the applicability of several mixing rules; e.g., see Wolff et al. (1998), Voshchinnikov & Mathis (1999), Chylek et al. (2000), and Voshchinnikov et al. (2005, 2006). The application of DDA poses a computational challenge, particularly for the high values of the size parameter $X(=2\pi a/\lambda > 20)$, and the complex refractive index m of the grain material would require large number of dipoles, and that in turn would require considerable computer memory and cpu time (see e.g. Saija et al. 2001; Voshchinnikov et al. 2006).

We also calculated the absorption efficiencies of the porous grains. Figure 6 shows the absorption efficiencies of the composite grains with the host silicate spheroids and voids as inclusions. It is seen that as the porosity increases i.e., as the volume fraction "f" of the voids increases, the peak strength decreases. However, we did not find any shift in the 10 μm and 18 μm features with porosity. Henning & Stognienko (1993) also did not find any change in the 10 μm or 18 μm feature for the porous silicate grains. Greenberg & Hage (1990) have shown the change in the feature strength and its shape with the porosity of the grain. Voshchinnikov et al. (2006) and Voshchinnikov & Henning (2008), have used a layered, sphered model to study the effect of porosity on the 10 μm feature, and they find that the peak strength decreases and the feature broadens with the porosity. Recently, Li et al. (2008) have used the porous grains to model the 10 μm feature in the AGN and they find a shift in the 10 μm absorption peak towards longer wavelengths. Min et al. (2007) have successfully used DDA to study the 10 μm silicate feature of fractal porous grains and explain the interstellar extinction in various lines of sight.

Figures 7–9 show the variation in absorption efficiencies with the grain sizes for the composite grains a = 0.05, 0.1, 0.5, and 1.0 μ, with the fraction of inclusion of ices, graphites, and voids respectively. It is seen that for the small sizes a = 0.05 and 0.1 μ, the variation in the absorption efficiency with the change in the volume fraction of inclusions is not appreciable, whereas the effect is clearly seen for the larger grains (a = 0.5 and 1.0 μ) i.e., absorption efficiency decreases with the increasing fraction of inclusions. In Fig. 8 we show the $Q_{\rm abs}$ for the silicate grain (i.e. volume fraction f = 0.00). There, the absorption is higher than for composite grains.

All these results on the composite grain models show variation in the absorption efficiencies with the variation in the volume fraction of the inclusions and porosities. These results also show that the peak absorption wavelength at 10 μm shifts with the graphite inclusions. These composite grain models do not show any shift in the absorption peak at 18 μm with the change in the volume fraction of the inclusions. Our results on

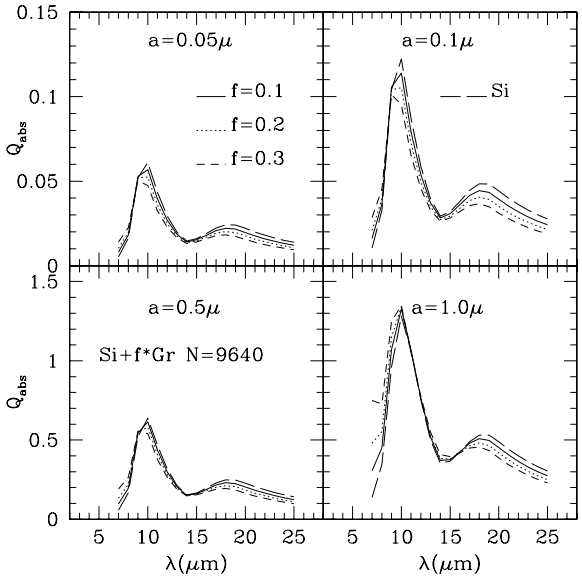

Fig. 8. Variation in absorption efficiencies with grain sizes. Host silicate spheroids contain dipoles, $N = 9640$, and graphites as inclusions. Also shown is the $Q_{\rm abs}$ for the silicate grain ($f = 0.0$) for all the sizes.

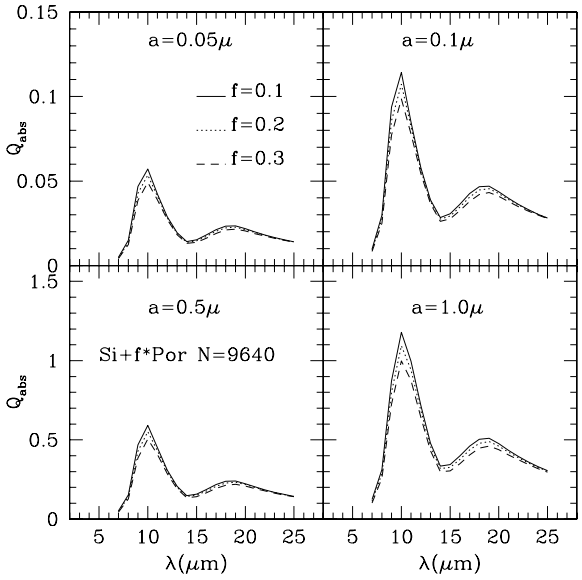

Fig. 9. Variation in absorption efficiencies with composite grain sizes. Host silicate spheroids contain dipoles $N = 9640$ and voids (vacuum) as inclusions.

the composite grain models do not show any broadening of the 10 μm or 18 μm feature.

3.2. Infrared emission from circumstellar dust: silicate features at 10 μm and 18 μm

In general, those stars which have evolved off the main sequence and that have entered the giant phase of their evolution are a major source of dust grains in the galactic interstellar medium. Such stars have oxygen overabundant relative to carbon and therefore produce silicate dust and show the strong feature at 10 μm. This is ascribed to the Si-O stretching mode in some form of silicate material, such as olivine. These materials also show a much

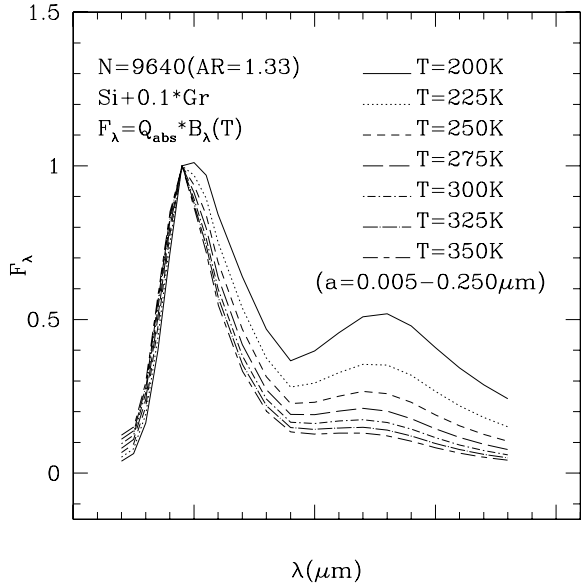

Fig. 10. Infrared flux at various temperatures for the composite grains with graphites as inclusions.

broader and weaker feature at 18 μm, resulting from the O-Si-O bending mode (Little-Marenin & Little 1990). Using the absorption efficiencies of the composite grains and a power-law MRN dust grain size distribution (Mathis et al. 1977), we calculate the infrared flux F_λ at various dust temperatures and compare the observed IRAS-LRS curves with the calculated infrared fluxes, F_λ for the composite grain models. The flux F_λ is calculated using the relation $F_\lambda = Q_{\rm abs} \cdot B_\lambda(T)$ at dust temperature T in K and B_λ as the Planck's function. This is valid only if the silicate emission region is optically thin (Simpson 1991; Ossenkopf et al. 1992; Li et al. 2008). Figure 10 shows the IR fluxes with various dust temperatures ($T = 200$–350 K) for the composite grains with $N = 9640$, and inclusions of graphites with $f = 0.1$ and MRN (Mathis et al. 1977) grain size distribution $a = 0.005$–0.250 μ. We checked the grain models with a larger grain size distribution ($a = 0.1$–1.0 μ) and found that it did not match the observed curve satisfactorily – the fit was very poor. Table 2 shows the best-fit χ^2 minimized values and corresponding temperatures for all the composite grain models with silicate host and graphite as inclusions. For details on χ^2 minimization please refer Vaidya & Gupta (1997, 1999). Table 3 shows the best fit χ^2 minimized values and corresponding temperatures for all the composite grain models with silicate host and voids (porous) as inclusions.

Figure 11a shows the average IRAS-LRS observed curve (Whittet 2003) and its comparison with the χ^2 minimized best-fit model $N = 9640$, $f = 0.1$ graphite inclusions and a temperature of $T = 270$ K. Figures 11b and c show the observed IRAS-LRS spectra of two typical stars that have strong silicate feature at 10 μ (IRAS class 6 as defined by Volk – see Olnon & Raimond 1986; Gupta et al. 2004) viz. IRAS 16340-4634 and IRAS 17315-3414. These two IRAS objects have been taken from the large set of 2000 IRAS spectra that were classified into 17 classes by eye (see Gupta et al. 2004) and that have the least problems with noise or spectral peculiarities. The first star IRAS 16340-4634 fits the χ^2 minimized model $N = 25\,896$ best, alongwith $f = 0.3$ graphite inclusions and a temperature of $T = 210$ K. The second star IRAS 17315-3414 best fits the χ^2 minimized model $N = 14\,440$, $f = 0.1$ graphites inclusions

Table 2. Minimum χ^2 values and corresponding temperatures (K in brackets) for Si+f*Gr composite grain models fitting the average IRAS-LRS observed IR flux, the two stars IRAS 16340-4634, IRAS 17315-3414, and three volume fractions of inclusions viz. f = 0.1, 0.2, and 0.3.

Average observed IRAS-LRS flux (Si+f*Gr)			
Inclusion fraction (f)	N = 9640	25 896	14 440
0.1	0.00249(270)	0.00260(270)	0.00391(290)
0.2	0.00273(265)	0.00332(260)	0.00450(280)
0.3	0.00410(260)	0.00573(260)	0.00596(275)
IRAS-LRS 16340-4634 flux (Si+f*Gr)			
0.1	0.00256(210)	0.00156(210)	0.00241(220)
0.2	0.00191(210)	0.00165(210)	0.00164(220)
0.3	0.00148(210)	0.00156(210)	0.00151(215)
IRAS-LRS 17315-3414 flux (Si+f*Gr)			
0.1	0.00814(230)	0.00846(235)	0.00798(245)
0.2	0.00972(230)	0.01112(230)	0.00985(240)
0.3	0.01251(230)	0.01474(230)	0.01256(240)

Table 3. Minimum χ^2 values and corresponding temperatures (K in brackets) for Si+f*Por composite grain models fitting the average IRAS-LRS observed IR flux, the two stars IRAS 16340-4634 and IRAS 17315-3414, and three volume fractions of inclusions viz. f = 0.1, 0.2, and 0.3.

Average observed IRAS-LRS flux (Si+f*Por)			
Inclusion fraction (f)	N = 9640	25 896	14 440
0.1	0.00387(290)	0.00442(300)	0.00526(310)
0.2	0.00472(305)	0.00575(320)	0.00613(325)
0.3	0.00570(315)	0.00708(340)	0.00713(340)
IRAS-LRS 16340-4634 flux (Si+f*Por)			
0.1	0.00400(220)	0.00427(220)	0.00450(225)
0.2	0.00451(220)	0.00505(225)	0.00517(230)
0.3	0.00543(220)	0.00599(230)	0.00591(230)
IRAS-LRS 17315-3414 flux (Si+f*Por)			
0.1	0.00644(245)	0.00629(245)	0.00660(250)
0.2	0.00615(245)	0.00599(250)	0.00655(255)
0.3	0.00609(250)	0.00625(260)	0.00661(260)

and a temperature of T = 245 K. Figures 12a–c are for the same IRAS-LRS average observed curve and the two IRAS stars respectively but best fitted to silicate host and voids (porous) as inclusions.

The results of model fits to the corresponding temperatures in Figs. 11 and 12 lie within a range of 210–290 K, which essentially indicates the expected range of dust temperatures in the circumstellar disks. One needs to compare the models with a larger set of observed spectra to make more definitive estimates of dust temperatures for individual IRAS and other sources (Henning & Stognienko 1993).

For the comparison with observed curves, we have not considered composite grain models with ice as inclusions. Ice is expected to condense in an O-rich stellar atmosphere if low enough temperature environments exist. Such conditions arise when the atmosphere is optically thick (Whittet 2003). Hoogzaad et al. (2002) have used core-mantle grain model with core silicate and ice as mantle to model the IR emission from the AGB star HD 161 796 and find that the core-mantle dust model with ice as mantle has a temperature in the range of 50–75 K.

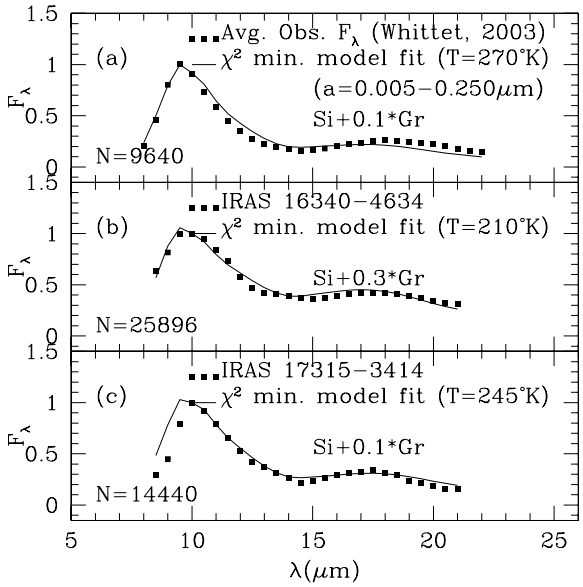

Fig. 11. Best fit χ^2 minimized composite grain models (silicates with graphite inclusions) plotted with the average observed infrared flux for the IRAS-LRS curve and the two stars, IRAS 16340-4634 and IRAS 17315-3414.

3.3. Flux ratio R = Flux(18 μ)/Flux(10 μ)

We also studied the effect of inclusions and porosity in the silicate grain on the flux ratio R = Flux(18 μ)/Flux(10 μ). Table 4 shows the ratio R for composite grain models with graphite (Si+f*Gr) and voids (Si+f*Por) as inclusions. This table shows that in general the ratio R decreases with the temperature, for both models and the ratio varies from ~0.6 at T = 200 K to ~0.2 at T = 300 K. It also shows that, for the composite grain models with graphite as inclusions, the ratio R decreases with the volume fraction of the inclusions, whereas for the models with the voids (i.e. porous grains), the ratio R increases with the volume fraction of voids. These results show that R increases with the porosity and thus clearly indicate that both the inclusions and porosities within the grains modify the emission features in the silicate grains. Henning & Stognienko (1993) did not find any variation in the ratio with the increase of the porosity. They also did not find any variation in the R with the inclusions of graphite.

Table 5 shows the ratio of silicate features R = Flux(18 μ)/Flux(10 μ) for the average IRAS-LRS observed curve, for the two stars mentioned above, and for the best fit corresponding models (from Figs. 11 and 12). It is seen from Table 5 that in general the model ratio R = Flux(18 μ)/Flux(10 μ) for the average observed curve (Whittet 2003) is lower than

Table 4. The ratio of silicate features R = Flux(18 μ)/Flux(10 μ) for composite grain models.

Si+f*Gr	9640			25 896			14 440		
T(K)	0.1	0.2	0.3	0.1	0.2	0.3	0.1	0.2	0.3
200	0.504	0.485	0.471	0.503	0.478	0.463	0.551	0.528	0.504
225	0.339	0.325	0.316	0.338	0.321	0.310	0.370	0.354	0.338
250	0.247	0.237	0.231	0.247	0.234	0.227	0.270	0.259	0.247
275	0.192	0.184	0.179	0.191	0.181	0.176	0.209	0.200	0.191
300	0.156	0.149	0.145	0.155	0.147	0.143	0.170	0.163	0.155
Si+f*Por	9640			25 896			14 440		
T(K)	0.1	0.2	0.3	0.1	0.2	0.3	0.1	0.2	0.3
200	0.567	0.592	0.619	0.584	0.620	0.655	0.607	0.631	0.656
225	0.381	0.398	0.416	0.392	0.416	0.439	0.408	0.423	0.440
250	0.278	0.290	0.303	0.286	0.304	0.321	0.298	0.309	0.321
275	0.215	0.225	0.235	0.220	0.236	0.249	0.231	0.240	0.249
300	0.175	0.183	0.191	0.180	0.191	0.202	0.187	0.194	0.202

Table 5. The ratio R = Flux(18 μ)/Flux(10 μ) for the models and observed silicate features.

Object/Star	R(Model Si+f*Gr)	R(Model Si+f*Por)	R(Observed)
Average Observed IRAS-LRS flux	0.201	0.189	0.255
IRAS 16340-4634	0.383	0.379	0.394
IRAS 17315-3414	0.276	0.283	0.236

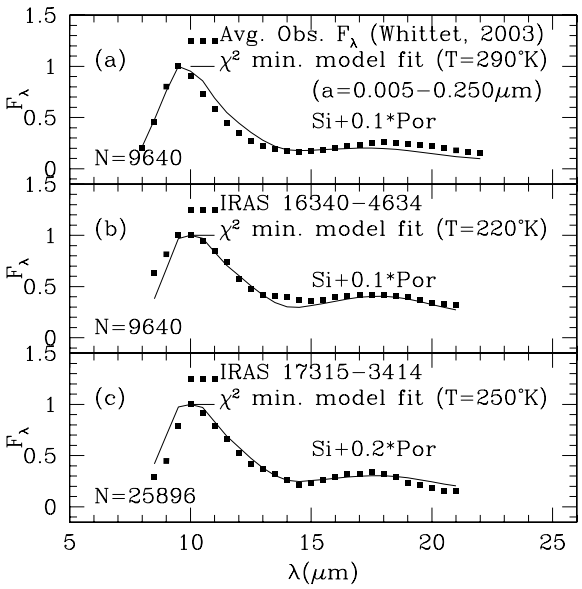

Fig. 12. Best fit χ^2 minimized composite grain models (silicates with porous inclusions) plotted with the average observed infrared flux for the IRAS-LRS curve and the two stars, IRAS 16340-4634 and IRAS 17315-3414.

obtained for the two stars IRAS 16340-4634 and IRAS 17315-3414. The model ratio, 0.383 for the star IRAS 16340-4634, is comparable to the one derived for the circumstellar dust i.e. 0.394 (Simpson 1991; and Ossenkopf et al. 1992). The low value of the ratio derived for the average observed circumstellar features may be due to O-deficient silicates as noted by Little-Marenin & Little (1990) and Ossenkopf et al. (1992). Ossenkopf et al. (1992) note that observationally determined flux ratio R for circumstellar dust varies from 0.3 to 0.6. However, the variation in R is not very significant if the range of R, 10 μm, and 18 μm features is considered. We need to compare the composite grain model with a larger sample of stars to interpret the R for various stellar environments as noted by Simpson (1991) & Henning & Stognienko (1993).

4. Comparison of our model/results with available model/results from other workers

In this section we make a detailed comparison of the results of our present work with several other published model/results on the silicate IR emission features, which are elaborated in Tables 6 and 7. For the discussion in these tables, the peak position of the 10 μm feature lies in the interval 9.5–10.2 μm and the $FWHM$ in the range of 1.8–3.2 μm, as derived by several authors, see Ossenkopf et al. (1992). It must be noted here that the list of composite and porous grain models given in Tables 6 and 7 are not exhaustive. We have included, particularly, the references/models that show variation in the 10 μm and 18 μm silicate features with volume fraction of inclusions or porosity.

These tables show that only three authors, Vaidya & Gupta (2010), Henning & Stognienko (1993), and Min et al. (2007), have used DDA for modeling the composite grains. Henning & Stognienko (1993) did not find any significant variation either in 10 μm, and 18 μm features or in the ratio R = Flux(18 μ)/Flux(10 μ) with porosity or inclusions. They also point out that the porous and composite grains are not the carriers of AFGL or BN objects. Min et al. (2007) have used a statistical ensemble of simple particle shapes to represent irregularly shaped particles, and the models fit the interstellar extinction profile in the spectral range of 5–25 μm. As mentioned earlier, the EMA methods used by others do not take into account the effects related to internal grain structure and grain surface roughness (see e.g. Henning & Stognienko 1993; Wolff et al. 1994; and Saija et al. 2001).

It must be emphasized that, in the present study, by using DDA for the composite grains, we have systematically studied the effects of inclusions and porosities and fit the IR emission from the circumstellar dust in the spectral range 5–25 μm. Further more, with our composite grain model, we fit the average observed IRAS-LRS emission curve obtained for circumstellar

Table 6. Comparison of our model/results with available model/results from other workers.

	Computational method	Particle shape	Inclusions/size and composition/ material	Specifications of model/method
Our work (2010)	DDA	Oblate	Inclusion size in terms of number of dipoles across the diameter Inclusion compositions are graphite/ice & vacuum (for porosity)	All composite grain models with volume fraction of inclusions viz. 10%, 20%, and 30% were studied
Lee & Draine (1985)	Rayleigh approximation	Oblate	Ice, Size: smaller than wavelength	Core-mantle grains
Jones (1988)	EMA[a] Hollow spheres	Spheres	Voids to model porous grains	Porosity 25% and 50%
Greenberg & Hage (1990)	EMA[a]	Spheres	Organic refractory material, Ice & voids	Inclusion of CHON particles to model cometary grains
Ossenkopf et al. (1992)	EMA[a]	Ellipsoids	Al2O3, MgO, MgS Fe3O4, Fe2O3, & amorphous carbon	10% inclusion of Al_2O_3, MgO, and MgS
Henning & Stognienko (1993)	DDA	Oblate and prolate The observed polarization across the 10 μm feature led them to conclude that the silicate particles are oblates rather than prolates	Inclusion size smaller than wavelength and inclusion composition consists of graphite, ice, voids, & amorphous carbon	Two fractions of inclusions Fsilicates/Fgraphites viz. 1.3 & 0.8
O'Donnell (1994)	EMA[a]	Oblates and prolates They found that prolate grains shift the 10 μm & 18 μm features too so as to be consistent with the observed data	Inclusion composition consists of amorphous carbon, glassy carbon, tholins, & voids	Core-mantle particles with silicate-amorphous ice and amorphous carbon
Min et al. (2007)	DDA	Gaussian random spheres Gaussian random field particles hollow spheres	Inclusion consists of distribution of amorphous carbon, amorphous silicate	Silicate grains with Mg component >0.9
Voshchinnikov & Henning (2008)	Layered[a] spheres	Spherical grains	Inclusion composition consists of amorphous carbon and amorphous silicates	Volume fraction of inclusions range from 0.2 to 0.9
Li et al. (2008)	Multi-layered[a] sphere model	Concentric spherical layers	Inclusion composition consists of amorphous carbon & porous/voids	Mass ratio of amorphous carbon v/s amorphous silicates to be ~0.7

Notes. [(a)] It is a mixture of two materials, there are no separate inclusions, size is not applicable.

dust around several M-type stars (Whittet 2003) and two other individual IRAS stars.

5. Summary and conclusions

We used the discrete dipole approximation (DDA) to calculate the absorption efficiency for the composite spheroidal grains and studied the variation in absorption efficiency with the volume fractions of the inclusions in the wavelength region of 5.0–25.0 μm. These results clearly show the variation in the absorption efficiency for the composite grains with both the volume fractions of the inclusions, and porosity. The results on the composite grains with graphite as inclusions show a shift towards shorter wavelength for the peak absorption feature at 10 μm with the volume fraction of the inclusions. However, these composite grain models did not show any shift in the 18 μm peak with the variation in the inclusions or porosities. Henning and Stognienko did not find any shift in either the 10 μm or the 18 μm feature for the oblate composite spheroid containing silicates and graphites. For the porous silicate grains, we did not find any shift in the 10 μm or 18 μm features, whereas Li et al. (2008) find the shift towards longer wavelength in the 10 μm feature for the porous silicate grains. Ossenkopf et al. (1992) found a shift towards shorter wavelength in the 10 μm feature for the composite silicate grains with carbon inclusions. The composite grain models presented in this study did not show any broadening in the 10 μm and 18 μm features. In Tables 6, 7 and Sect. 4, we compare and summarize all the results.

The dust temperatures between 200–350 K derived from the composite grain models fit with the observed IRAS-LRS curve and are comparable to the dust temperature range 200–400 K as suggested by Voshchinnikov & Henning (2008). The ratio

Table 7. Comparison continued from previous table.

	Characteristics of 10 μm feature	Characteristics of 18 μm feature	Ratio(R) 18 μm/10 μm	Observational characteristics
Our work (2010)	Shifts shortwards with graphite inclusions & no broadening of this feature is indicated	No shift in this feature is indicated	R Decreases with volume fractions of graphite; increases with porosity & varies between 0.2–0.6	Dust temperatures 200–350 K are derived from composite grain models fit the observed IRAS-LRS curve as well as for 2 stars selected in this paper
Lee & Draine (1985)	No shift is indicated	Not studied	R not determined	Core-mantle grain model fit well with the observed IR emission from BN object
Jones (1988)	Feature is enhanced	Feature is enhanced	R not determined	No comparison was made
Greenberg & Hage (1990)	Grains with silicate cores & refractory organic materials as mantles with ~60–80% porosity fit the 10 μm feature observed in comets	This feature was not studied	R not determined	Pure silicate does not fit the observed emission in comets but porous grains and CHON particles fit the observed IR emission from cometary dust
Ossenkopf et al. (1992)	Feature shifts shortwards (~0.3 μm) & broadens ($FWHM$ 2–2.7 μm) with Al2O3 inclusions	Did not find any shift in this feature	$R \sim 0.3$–0.5 for most inclusions & is enhanced to 0.68 for MgO	Grain models based on optical constants of astronomical Si (Draine 1985) do not fit the observed observed IR emission from circumstellar dust
Henning & Stognienko (1993)	No appreciable shift with inclusions indicated	Feature shifts shortwards and broadens with amorphous carbon	$R \sim 0.41$–0.47	Porous and composite grains do not fit the observed IR emission from AFGL 2591 or BN objects
O'Donnell (1994)	No shift in this feature with inclusions indicated	No shift in this feature with inclusions is indicated	$R = 0.51$ for prolates $R = 0.42$ for oblates Observed R value is between 0.3–0.6	The silicate grains which give rise to the 10 μm & 18 μm features do not posses any coatings of amorphous or glassy carbon
Min et al. (2007)	Feature shifts shortwards (~0.5 μm) & broadens ($FWHM$ 2–2.5 μm)	No shift in this feature	R not determined	GRF, DHS and irregularly shaped particles fit the interstellar spectrum in the region 5–25 μm
Voshchinnikov & Henning (2008)	The strength of this feature decreases with the porosity and the feature also broadens ($FWHM$ 2.1–2.7 μm)	This feature was not studied	R not determined	Porous and fluffy grain models fit the observed 10 μm feature in T-Tauri & Herbig Ae/Be stars
Li et al. (2008)	This feature shifts to longer wavelengths (~10.6 μm) & the profile broadens ($FWHM$ 2.1–2.8 μm) with porosity	This feature was not studied	R not determined	Observed 10 μm feature can be explained in terms of porous composite dust consisting of amorphous Si and C & vacuum

R = Flux(18μ)/Flux(10 μ) obtained from the composite grain model varies from 0.2 to 0.6 and compares well with the one derived from the observed IRAS-LRS curves for the circumstellar dust; see Little-Marenin & Little (1990), Ossenkopf et al. (1992), and Volk & Kwok (1988).

It must be noted here that the composite grain models considered in the present study are not unique. However, these results for composite grains clearly indicate that the silicate features at 10 μm and 18 μm vary with the volume fraction of inclusions and porosities. We also note that the results based on DDA and EMA calculations for the composite grains do not agree. The composite grain models presented in this paper need to be compared with a larger sample of stars with circumstellar dust (Little-Marenin & Little 1990; Simpson 1991; Ossenkopf et al. 1992; Henning & Stognienko 1993).

Acknowledgements. D.B.V. and R.G. thank ISRO-RESPOND for the grant (No. ISRO/RES/2/345/ 2007-08) under which this study has been carried out. Authors thank the referee for constructive suggestions.

References

Bazell, D., & Dwek, E. 1990, ApJ, 360, 342
Bohren, A., & Huffman, J. B. 1983, in Absorption and Scattering of Light by Small Particles (New York: John Wiley & Sons Inc.)
Chylek, P., Videen, G., Geldart, D. J. W., Dobbie, J., & William, H. C., 2000, in Light Scattering by Non-spherical Particles, ed. M. Mishchenko, J. W. Hovenier, & L. D. Travis (New York: Academic Press), 274
Dobbie, J. 1999, Ph.D. Thesis, Dalhousie University
Draine, B. T. 1985, ApJS, 57, 587
Draine, B. T. 1987, Preprint Princeton Observatory, No. 213
Draine, B. T. 1988, ApJ, 333, 848
Draine, B. T., & Flatau, P. J. 2003, DDA code version "ddscat6"
Greenberg, J. M., & Hong, S. S. 1975, The Dusty Universe, ed. N. Watson (Acad. Publ), 132
Gupta, R., Singh, H. P., Volk, K., & Kwok, S. 2004, ApJS, 152, 201

Gupta, R., Mukai, T., Vaidya, D. B., Sen, A. K., & Okada, Y. 2005, A&A, 441, 555
Gupta, R., Vaidya, D. B., Dobbie, J. S., & Chylek P. 2006, Ap&SS, 301, 21
Greenberg, J. M., & Hage, J. 1990, ApJ, 361, 251
Henning, Th., & Stognienko, R. 1993, A&A, 280, 609
Hoogzaad, S., Molster, F., & Dominik, C. 2002, A&A, 389, 547
Iati, M. A., Giusto, A., Saija, R., et al. 2004, ApJ, 615, 286
Irvine, W. M., & Pollack, J. B. 1968, ICARUS, 8, 324
Jones, A. P. 1988, 234, 209
Lee, H. M., & Draine, B. T. 1985, ApJ, 290, 211
Li, M. P., Shi, Q. J., & Li, A. 2008, MNRAS, 390, 778
Little-Marenin, J. R., & Little, S. J. 1990, AJ, 94, 1173
Mathis J. S. 1996, ApJ, 472, 643
Mathis, J. S., & Whiffen, G. 1989, ApJ, 341, 808
Mathis, J. S., Rumpl, W., & Nordsieck, K. H. 1977, ApJ, 217, 425
Min, M., Dominik, C., Hovenier, J., deKoter, A., & Waters, L. A. F. M. 2006, A&A, 445, 1005
Min, M., Waters, L. A. F. M., deKoter, A., et al. 2007, A&A, 462, 667
Mishchenko, M. L., Travis, L. D., & Lacis, A. A. 2002, in Scattering, Absorption and Emission of Light by Small Particles (Cambridge, UK: CUP), 184
O'Donnell, J. E. 1994, ApJ, 437, 262
Olnon, F. M., & Raimond, E. 1986, A&AS, 65, 607
Ossenkopf, V. 1991, A&A, 251, 210
Ossenkopf, V., Henning, Th., & Mathis, J. 1992, A&A, 261, 567
Perrin, J. M., & Lamy, P. L. 1990, ApJ, 364, 146
Perrin, J. M., & Sivan, J. P. 1990, A&A, 228, 238
Purcell, E. M., & Pennypacker, C. R. 1973, ApJ, 186, 705
Saija, R., Iati M., Borghese, F., Denti, P., Aiello, S., & Cecchi-Pestellini, C. 2001, ApJ, 539, 993
Simpson, J. P. 1991, ApJ, 368, 570
Vaidya, D. B., & Gupta, R. 1997, A&A, 328, 634
Vaidya, D. B., & Gupta, R. 1999, A&A, 348, 594
Vaidya, D. B., & Gupta, R. 2009, JQSRT, 110, 1726
Vaidya, D. B., Gupta, R., Dobbie, J. S., & Chylek, P. 2001, A&A, 375, 584
Vaidya, D. B., Gupta, R., & Snow T. P. 2007, MNRAS, 379, 791
Volk, K., & Kwok, S. 1988, ApJ, 331, 435
Voshchinnikov, N. V., & Henning, Th. 2008, A&A, 483, L9
Voshchinnikov, N. V., & Mathis, J. S. 1999, ApJ, 526, 257
Voshchinnikov, N. V., Il'in, V. B., & Henning, Th. 2005, A&A, 429, 371
Voshchinnikov N. V., Il'in V. B., Henning, Th., & Dobkova D. N. 2006, A&A, 445, 993
Whittet, D. C. B. 2003, in Dust in the Galactic Environments, 2nd edn. (UK: IOC Publishing Ltd.), 125
Wolff, M. J., Clayton, G. C., Martin, P. G., & Sculte-Ladlback, R. E. 1994, ApJ, 423, 412
Wolff, M. J., Clayton, G. C., & Gibson, S. J. 1998, ApJ, 503, 815